OVERVIEW OF FRACTAL CLOUDS

Robert F. Cahalan
Laboratory for Atmospheres
NASA Goddard Space Flight Center
Greenbelt, Maryland 20771, USA

ABSTRACT

We summarize work being done at the Goddard Laboratory for Atmospheres on the fractal properties of clouds and their effects on the large-scale radiative properties of the atmosphere. This involves three stages:

1. analysis of high resolution cloud data to determine the scaling properties associated with various cloud types;
2. simulation of fractal clouds with realistic scaling properties;
3. computation of mean radiative properties of fractal clouds as a function of their scaling properties.

The approximation that clouds are scaling fractals with dimension 4/3 (Lovejoy, 1982) must be modified in three ways: First, a change in the fractal dimension is found at a characteristic size which depends upon cloud type, so that exact scale invariance does not hold. Secondly, the fractal dimensions are different for each cloud type in a given size range, so that exact universality does not hold. Finally, the more intense cloud areas are found to have a higher perimeter fractal dimension, perhaps indicative of the increased turbulence at cloud top.

Simulations of fair weather cumulus and stratocumulus clouds have been developed which take these properties into account. The simulations depend upon two scaling parameters which determine the distributions of cloud sizes and spacings, respectively, and also upon a maximum characteristic cell size.

The initial Monte Carlo radiative transfer computations have been carried out with a highly simplified model in which liquid water is redistributed in an initially plane-parallel cloud while cloud height and mean optical depth are held fixed. Redistribution decreases the mean albedo from the plane parallel case, since the albedo of optically thick regions saturates as optical depth is increased. The albedo of each homogeneous region may be computed from the thickness of each region independently only when the horizontal optical depth is large compared to the photon mean free path. The albedo of a region comparable in horizontal optical depth to the photon mean free path depends upon radiation from the sides. The mean albedo is insensitive to variations in optical depth on horizontal scales much smaller than the photon mean free path. These concepts have been illustrated with a simple one-parameter fractal model.

RSRM '87: ADVANCES IN
REMOTE SENSING RETRIEVAL METHODS
A. Deepak, H.E. Fleming, and J.S. Theon (Eds.)

ISBN 0-937194-13-1

1. INTRODUCTION

There is a growing body of observational evidence on inhomogeneous cloud structure. Derr and Gunter (1982) reported searching in vain for the sort of clouds assumed by cloud radiation modelers (whether plane-parallel, or a lattice of simple shapes). More recently, measurements of vertically averaged liquid water at one-minute intervals over a three-week period during the July 1987 FIRE experiment at San Nicolas Island in California stratus -- perhaps the closest thing to plane-parallel clouds -- show variations on all scales (J. B. Snider, private communication). Baker and Latham (1979) have suggested that such variations arise from inhomogeneous entrainment. Entrained dry air, rather than mixing uniformly with cloudy air, remains intact in blobs of all sizes, which decay only slowly by invasion of cloudy air.

A useful notion for discussing such cloud structure is that of a "scaling fractal" (Mandelbrot, 1983 and references therein), which is a set or object which is extremely irregular on all scales, while at the same time statistically invariant under certain transformations of scale. The simplest examples are the statistically "self-similar" fractals (op.cit. p. 350) -- geometrical patterns (other than Euclidean lines, planes and surfaces) with no intrinsic scale, so that no matter how closely you inspect them, they always look the same, at least in a statistical sense. While self-similar fractals are statistically isotropic, the so-called "self-affine" fractals scale differently in different directions (see e.g. Mandelbrot, 1986). The most general scaling fractals are the multidimensional fractals, or "multifractals" (Hentschel and Procaccia, 1983 and Frisch and Parisi, 1985) which exhibit a spectrum of fractal dimensions.

Lovejoy (1982) has presented empirical evidence that clouds are statistically self-similar in the horizontal plane from 1000 km down to 1 km, with a fractal dimension of approximately 4/3. If this were strictly true, than a satellite image of a cloud field, taken over a uniform dark ocean background with no evident geographical features, would be statistically indistinguishable from an image of any small portion of the scene if it had the same number of pixels as the original. Schertzer and Lovejoy (1986) have argued that clouds are self-affine in a vertical plane, and have considered multifractal cloud models (Schertzer and Lovejoy, 1988 and references therein). These idealizations provide important alternatives to the simple plane-parallel or lattice cloud fields, and it is important to consider their consequences and limitations.

The purpose of this paper is to give a brief summary of work being done at the Goddard Laboratory for Atmospheres to investigate the implications of the fractal properties of clouds for the large-scale radiative properties of the atmosphere. The empirical work is being done in collaboration with Mark Nestler of Science Applications Research, and Professor J. H. Joseph and his group at Tel-Aviv University. The radiative transfer computations are being done in collaboration with Warren Wiscombe of Goddard and William Ridgeway of Applied Research Corporation. Our approach involves three stages:

1. analysis of high-resolution cloud data to determine the spatial structure of various cloud types;
2. simulation of the spatial distribution of cloud liquid water and optical depth using a minimum number of parameters; and
3. computation of the mean radiative properties of the simulated clouds as a function of the cloud parameters.

The outline of the paper will follow these three stages. In the next section we begin by giving a brief introduction to fractals with a few simple examples. Section 3 summarizes the results of the analysis of LANDSAT data. Section 4 discusses a simple class of cloud simulations. Section 5 discusses the radiative properties of the simplest simulated cloud having a single fractal parameter. Finally, section 6 concludes with a brief discussion.

2. INTRODUCTION TO FRACTALS

A fractal is a mathematical set or object whose form is extremely irregular and/or fragmented on all scales. Clouds certainly qualify under this general but rather vague definition. To become more concrete and specific, we consider a self-similar scaling fractal, which is an object which remains similar (in the sense of statistical distributions) when subject to arbitrary magnification. (Fractals invariant under non-isotropic rescalings are termed self-affine.) Statistical properties such as the power spectrum, P, scale as

$$P(\lambda x) = \lambda^{f(d)} P(x), \tag{2.1}$$

where f is a scaling exponent which depends upon the fractal dimension d, which may be defined in terms of N_i, the number of objects with characteristic linear dimension r_i, as

$$N_i = C/r_i^d, \tag{2.2}$$

where C is a constant of proportionality. For a discussion of various types of dimensions in the context of chaotic attractors see Farmer et al., 1983.

In the following we give three simple examples of fractals, each introducing a new aspect needed in the fractal modelling of clouds. For a more systematic mathematical discussion of fractal sets, see Falconer (1985).

Perhaps the simplest example of a fractal is the von Koch snowflake. In order to construct this, we define a "kink operator" K, which puts a kink in every straight line segment of any figure by replacing its middle third by two equal line segments:

$$K(\text{——}) = \text{—}\Lambda\text{—} \tag{2.3}$$

The snowflake is generated from an equilateral triangle by successive applications of K. The first application, $K(\Delta)$, produces a figure with $3*4 = 12$ sides, each 1/3 as long as the sides of the original triangle. After n applications, $K^n(\Delta)$ has $3*4^n$ sides, each $1/3^n$ as long as the original, so that the perimeter is $3*(4/3)^n$. In the limit $n \to \infty$ of $K^n(\Delta)$, the fractal snowflake, $K^\infty(\Delta)$, has an infinite perimeter which encloses a finite area! Even in this simplest example, we see that fractals force us to modify our usual intuitions about geometrical objects.

The kink operator explicitly generates the multiple scales of a fractal, but the iteration of even the simplest operator may generate multiple scales, even when this is not explicit in the operator. Mandelbrot demonstrated this with the simple quadratic function. Consider the "Mandelbrot operator"

$$M(z) = z^2 + c, \tag{2.4}$$

where z and c are complex. For each value of c, we begin at $z_0=0$ and iterate, computing $z_1=M(0)$, then $z_2=M(M(0))$, and so on. The Mandelbrot Set consists of those values of c for which $z_\infty < \infty$. It is a compact set with a fractal boundary. Zooming in on the boundary, one sees miniature copies of the whole set which are roughly similar, just as in the snowflake. Unlike the snowflake, however, each copy has its own unique features, and increasingly complex structures appear as one zooms in. The iteration process is analogous to a dynamical process, with the operator M generating the time evolution from the initial state at z_0. The fact that such a complex attractor arises from a mapping as simple as (2.4) suggests the ubiquity of fractals in dynamical systems.

Neither of the above two examples contain any random element, which is necessary in the modelling of clouds. Thus as a final example in our list of "simplest" fractals, consider a random walk on a one-dimensional lattice with unit lattice spacing. In the usual non-fractal random walk, only nearest-neighbor jumps are allowed, and if both directions are equally probable, the probability of making a transition Δx is given by

$$p(\Delta x) = 1/2[\delta_{\Delta x,1} + \delta_{\Delta x,-1}], \tag{2.5}$$

and the corresponding structure function, the Fourier transform of (2.5), is

$$p(k) = \cos(k), \tag{2.6}$$

where k is the wavenumber. All other quantities of interest may be computed in terms of p(k). In particular, the single particle distribution becomes Gaussian at large times, with a variance increasing linearly with time, the well-known diffusion law.

To generate a fractal random walk, termed a "Levy walk" (Shlesinger, West and Klafter, 1987, and references therein) we allow not only nearest-neighbor jumps, but also jumps of length b with probability 1/a, jumps of length b^2 with probability $1/a^2$, and so on, where a and b are integers greater than 1. The transition probability then becomes

$$p(\Delta x) = (a-1)/2a \sum_{n=0}^{\infty} 1/a^n[\delta_{\Delta x,b^n} + \delta_{\Delta x,-b^n}], \tag{2.7}$$

and the corresponding structure function is

$$p(k) = (a-1)/2a \sum_{n=0}^{\infty} 1/a^n \cos(b^n k). \tag{2.8}$$

This distribution is identical to Weierstrass' example of a function which is continuous, but nowhere differentiable. If the time required for each jump is assumed to be an increasing function of the jump distance, the variance of the single particle distribution at large times increases as a power greater than one, which Shlesinger et al. have termed "enhanced diffusion".

The record of a single realization of a Levy walk shows a property also seen in cloud fields : a heirarchy of clusters (Randall and Huffman, 1980 and Cahalan, 1986). A

typical particle initially takes a number of nearest-neighbor jumps, then a larger jump of size b followed by more nearest-neighbor jumps, and so on, until eventually a jump of size b^2 occurs. After a number of b^2 jumps occur, there will eventually be a b^3 jump, and so on. Any given cluster of points, then, is part of a larger cluster created by the less frequent events.

3. EMPIRICAL RESULTS

The initial finding of Lovejoy (1982) that clouds are self-similar fractals was based upon a scatter plot of the area versus the perimeter of cloud areas determined by a threshold method from meteorological satellites and radar. This study was limited to clouds larger than a kilometer or so in horizontal dimension. Lovejoy and Mandelbrot (1985) studied the distribution of rain areas in GATE and compared them to a "fractal sum of pulses" (FSP) model. Lovejoy and Schertzer (1985) found somewhat better agreement with a "scaling cluster of pulses" (SCP) model, and Rhys and Waldvogel (1986) found violations of scaling in hail clouds. We have extended these results by employing the finer resolution available in LANDSAT data (see for example Cahalan, 1987, Cahalan and Joseph, 1988, and Wielicki and Welch, 1986.) We give a brief summary of the LANDSAT findings below.

In analysis of a large number of LANDSAT multispectral scanner (MSS) and thematic mapper (TM) images, over 200,000 cloud areas were identified. The procedure was to first determine the cloud fraction from the thermal channel by the spatial coherence method (Coakley and Bretherton, 1982). The brightness threshold was then adjusted to give the same cloud fraction in the reflected channels. This was termed the cloud "base" threshold. The method works well for the fair weather cumulus and stratocumulus clouds upon which the study focused, but fails for thin cirrus which show up only in the thermal channel. All contiguous areas above the threshold were identified for each scene. Finally, a second cloud "top" threshold was chosen in such a way that the brighter areas covered approximately 10% of the cloud fraction.

The distribution of cloud areas was first determined by binning in terms of the logarithm of the square root of the area, and plotting the logarithm of the number in each bin. If we let

$$r_i = (A_i)^{1/2}, \tag{3.1}$$

where A_i is the cloud area, then if clouds are scaling fractals we expect a power-law $N_i = C/r_i^p$, which gives

$$\log(N_i) = \text{constant} - p \log(r_i), \tag{3.2}$$

so that the log-log plot should be linear with slope -p. In fact, we typically found two linear regions separated by a sharp break in slope at a characteristic size which is about 0.5 kilometers for fair weather cumulus. The smaller clouds follow the straight line quite closely, with a slope typically p=0.6.

Scatter plots of cloud perimeter versus the square root of the area on a log-log plot show a change in slope at the same characteristic scale. The smaller fair weather cumulus follow a slope close to Lovejoy's value of 4/3, but the larger fair weather cumulus have an average slope of 1.55.

The fact that the larger clouds are less probable and more irregular in shape suggests a random coincidence hypothesis. That is, the smaller clouds are generated by a scaling fractal process up to some maximum cell size of about 0.5 kilometers, and larger clouds occur only as accidental coincidences of the smaller ones. One test of this picture is to see if the smaller cloud areas have a simpler distribution of cloud brightnesses within each cloud area. Visual inspection of a few scenes seems to bear this out, since we observe that the smaller cloud areas have a single brightness maximum, while larger ones invariably have multiple brightness maxima.

Raising the threshold to a high level allows the determination of the fractal dimensions of the bright regions, those above the cloud "top" threshold. The brighter regions were found to have higher perimeter dimensions for both fair weather cumulus and stratocumulus. In the case of fair weather cumulus it may be that the thicker, and therefore brighter, cloud regions are more irregular because they arise from the random coindidence of the smaller cells. On the other hand, in the case of stratocumulus this may be associated with increased turbulence at the cloud top, where the convection is driven by radiative cooling (Caughey et al., 1982). Note that there is a limit to the increase of the perimeter dimension with threshold, since the brighter regions cover a successively smaller area as the threshold is raised.

Stratocumulus dimensions are intermediate between the smaller and larger fair weather cumulus, and the break in slope is less pronounced. Since stratocumulus convection is driven by cooling at the cloud top, rather than heating from below as in fair weather cumulus, the stratocumulus downdraft regions are of special interest. These take the form of long, irregular leads, not unlike those observed in sea ice.

The mean radiative properties of a cloud field depend not only on the shapes of individual cloud areas, but also upon the relative spatial arrangement of the clouds. Perhaps the simplest measure of this is the distance from the center of a given cloud to that of its nearest neighbor. One can show (Cahalan, 1986) that cloud centers distributed randomly and independently would produce a Weibull-type nearest-neighbor distribution, which is sharpley peaked near the mean spacing, so that large cloud clusters separated by large gaps have exponentially small probability. By contrast, the spacing of cumulus clouds in the LANDSAT images shows many large gaps and clusters. While a Weibull-type distribution is an adequate fit for small spacings, the larger spacings are better fit by a distribution generated by a Levy walk similar to that discussed above.

To summarize our empirical results:

1. the horizontal scaling properties of clouds depend upon characteristic sizes (e.g. larger fair weather cumulus are more irregular), cloud type (stratocumulus are more irregular than small fair weather cumulus), and brightness threshold (brighter regions being more irregular).
2. the greater irregularity of larger clouds and brighter regions of cloud suggest a hypothesis of random coincidence of smaller cloud elements.
3. cloud spacings are not independently distributed, but exhibit strong clustering similar to that of a Levy walk.

4. CLOUD SIMULATIONS

In the preceeding section we drew a number of conclusions about cloud structure based on observations of cloud reflectivity. What we really wish to know is how the cloud liquid water is distributed, since the reflectivity is computable from the distribution of liquid water, traditionally by specifying microscopic properties like drop sizes, and macroscopic properties like optical depth, etc.. As we shall see in the next section, the radiation field provides a kind of low-pass spatial filter, so that there may be small-scale variations of liquid water to which the LANDSAT data is completely insensitive. Analysis of data on cloud liquid water during the FIRE field program should help pin down the important relationship between reflectivity and liquid water.

For the sake of this discussion, we must assume a distribution of liquid water which depends upon a few basic input parameters, and then determine output parameters from the resulting reflectances which may be compared with the LANDSAT results. Let us consider the minimum set of parameters needed to describe the reflectivity of a fair weather cumulus cloud field :

$$\begin{aligned} &\alpha_r = 0.6, \text{ power of the } \sqrt{\text{area distribution,}} \\ &A_r = (1/2 \text{ km})^2, \text{ maximum area,} \\ &\\ &\beta_r = 1.6, \text{ power of the spacing distribution,} \\ &x_r = 1 \text{ km, maximum spacing,} \end{aligned} \qquad (4.1)$$

where the subscript reminds us that these are parameters of the reflectivity field. We assume that the distribution of the square root of the area falls off with a power of -0.6 out to an area of 0.5 km, and that the nearest-neighbor spacing is determined by a Levy walk with a power of 1.6 out to a maximum spacing of 1 km. Larger cloud areas and larger spacings are assumed to occur by random coincidences.

One procedure for generating a field of liquid water which can reproduce the above parameters is as follows :

1. choose some simple initial distribution of liquid water, such as a homogeneous ellipsoid, which we shall term a "zero generation cloudlet", labelled c_0;
2. choose a power, α_{lw}, for the distribution of cloudlet horizontal size, so that the probability density of size goes as $(\text{size})^{-\alpha_{lw}}$ out to some specified maximum size, and let the orientations be uniformly distributed;
3. choose a power, β_{lw}, for the distribution of cloudlet horizontal spacings, so that the probability density of spacings goes as $(\text{spacing})^{-\beta_{lw}}$ out to some specified maximum spacing, and let the direction to the neighboring cloudlet be distributed isotropically;
4. generate a "first generation cloudlet" from the zero generation one, $c_1 = F(c_0)$, by superimposing c_0 cloudlets with sizes and spacings chosen from the above distributions, and successive locations being generated by a Levy walk; where cloudlets overlap, the liquid water is added up until a "saturation" value is reached, and the cloudlet in which saturation first occurs is defined to be c_1;
5. iterate the above, so that $c_2 = F(F(c_0))$, and so on.

As a result of the iteration, the liquid water field eventually becomes insensitive to details of the c_0 cloudlet, but depends upon the parameters of the size and spacing distributions. Parameters of the associated reflectivities, computed by Monte Carlo methods, also depend upon the liquid water parameters. They must be adjusted to reproduce (4.1), so that for example $\alpha_r(\alpha_{lw},A_{lw},\beta_{lw},x_{lw})=0.6$.

Even this minimal attempt to reproduce the LANDSAT analysis involves a number of parameters, and the Monte Carlo computation introduces additional parameters, as we shall see in the next section. For the sake of theoretical simplicity in understanding the radiative results, it is useful to introduce a highly simplified fractal cloud model involving a single fractal parameter.

Our simplified fractal liquid water distribution has a constant mean vertical optical depth, $\tau_v(0)$, and a constant mean horizontal optical depth, $\tau_h(0)$. We begin with a plane parallel cloud which is infinite in one horizontal direction and has, for example, $\tau_h(0) = 4000$ in the other horizontal direction, and $\tau_v(0) = 10$ in the vertical. The cloud is then divided horizontally in half, and one of the halves is chosen at random in which τ_v is increased by a factor, say $f = 0.3$, while τ_v is decreased by the same factor in the other half. The total amount of liquid water and the mean optical depth remain unchanged. The cloud thickness is also kept fixed, so that the changes in τ_v are due to changes in the droplet density alone, and may be thought of as a transfer of droplets from one half to the other. Each half is then subdivided again in half, and the same process of droplet transfer carried out in each half, so that one has 2^2 regions, each with

$$\tau_h(2) = (1\pm f)(1\pm f)\tau_h(0)/2^2, \text{ and}$$
$$\tau_v(2) = (1\pm f)(1\pm f)\tau_v(0). \qquad (4.2)$$

where the + and - signs occur with equal probability. The sum of all the values of $\tau_h(2)$ equals $\tau_h(0)$, so that the average horizontal optical depth is $\tau_h(0)/2^2$. The average vertical optical depth is of course $\tau_v(0)$. This subdivision process is then iterated down to a small "inner scale". In the above example the average τ_h is reduced to about one after twelve iterations, at which point τ_v varies between about 0.1 and 10 (see e.g. figure 1). The wavenumber spectrum of τ_v is approximately a power-law, with a power depending on f (see next section).

Figure 1 shows a horizontal cross-section of the vertical optical depth variations for one realization of the subdivision process described above. The optical depth is uniform in the perpendicular plane. The cloud height and the droplet size distribution are assumed constant, so that these variations may be thought of as variations in droplet density only. In the next section we discuss Monte Carlo radiative transfer computations for this highly simplified fractal cloud.

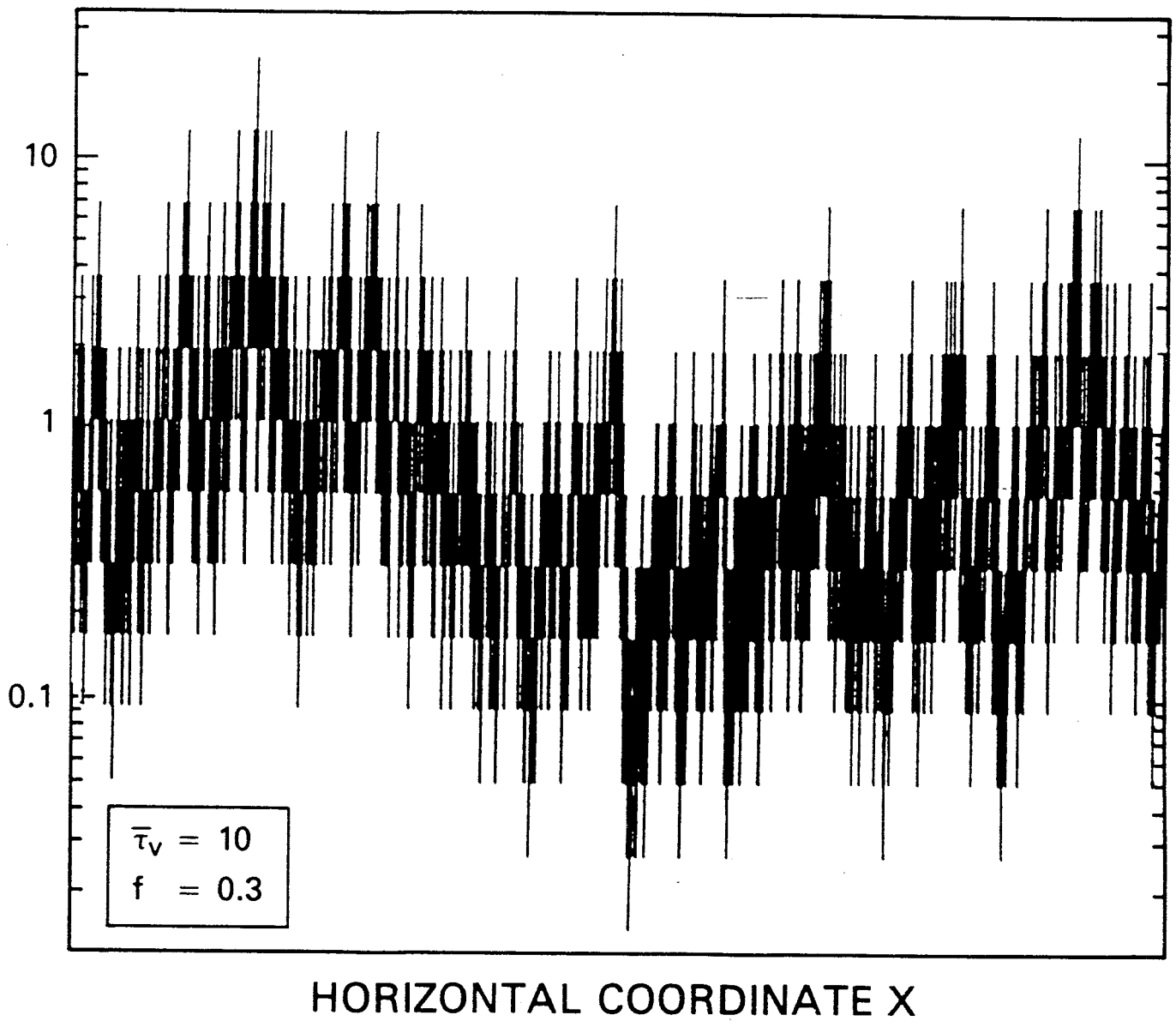

Figure 1. One realization of the horizontal variation of optical depth for the subdivision process described in the text after 12 iterations. (The optical depth is uniform in the other horizontal direction.) The initial horizontal optical depth of 4000 has been divided into 2^{12}=4096 segments with average horizontal optical depth of about 1 and vertical optical depth varying from about 0.1 to 10. The mean vertical optical depth is 10, and does not vary during the iteration.

5. MONTE CARLO COMPUTATIONS

The radiative transfer results described in this section are from Wiscombe et al. (1988). Although the results depend on only a single fractal parameter, the parameter f described in the preceeding section, there are additional parameters associated with the iteration process, and with the Monte Carlo computation itself. We first list the input parameters associated with the optical depth variations, along with our "typical values" :

1. $f = 0.3$: fractal parameter;
2. $\tau_h(0) = 4000$: initial horizontal optical depth;
3. $N = 12$: number of iterations;
4. $NR = 10$: number of realizations
5. $NP = 80{,}000$: number of photons per realization;

and finally we list the input parameters in common with the usual one-dimensional radiative computations :

6. $\tau_v(0) = 10$: mean vertical optical depth;
7. $\omega_0 = 1$: single scattering albedo;
8. $\theta = 60°$, $\phi = 0°, 180°$: sun angle;
9. $g = 0.85$: asymmetry parameter (Henyey-Greenstein phase function)

The power spectrum of the subdivision process may be determined from the covariance, which may be computed as follows: If, after N subdivisions, we let R be the ratio of vertical optical depth at some typical point to the mean vertical optical depth, $R=\tau_v(N)/\tau_v(0)$, then it is a product of N factors $1\pm f$, and the logarithm

$$\ln(R) = \sum_{k=1}^{N} x_k \tag{5.1}$$

is a sum of N independent identically distributed random variables, $x_k = \ln(1\pm f)$, and is therefore normally distributed for large N. If we consider two points separated by distance d, they will become separated into two segments after, say, n steps, where n is determined by

$$n = \{\text{smallest } k \ni d \geq L/2^k\}. \tag{5.2}$$

where L is the horizontal length corresponding to $\tau_h(0)$. The covariance may be determined using the two identities

$$R_1 R_2 = \exp[\ln R_1 + \ln R_2], \tag{5.3}$$

and

$$\langle \exp[y] \rangle = \exp[\langle y \rangle + \mathrm{var}(y)/2], \tag{5.4}$$

where angular brackets indicate an ensemble average, and y is any normally distributed

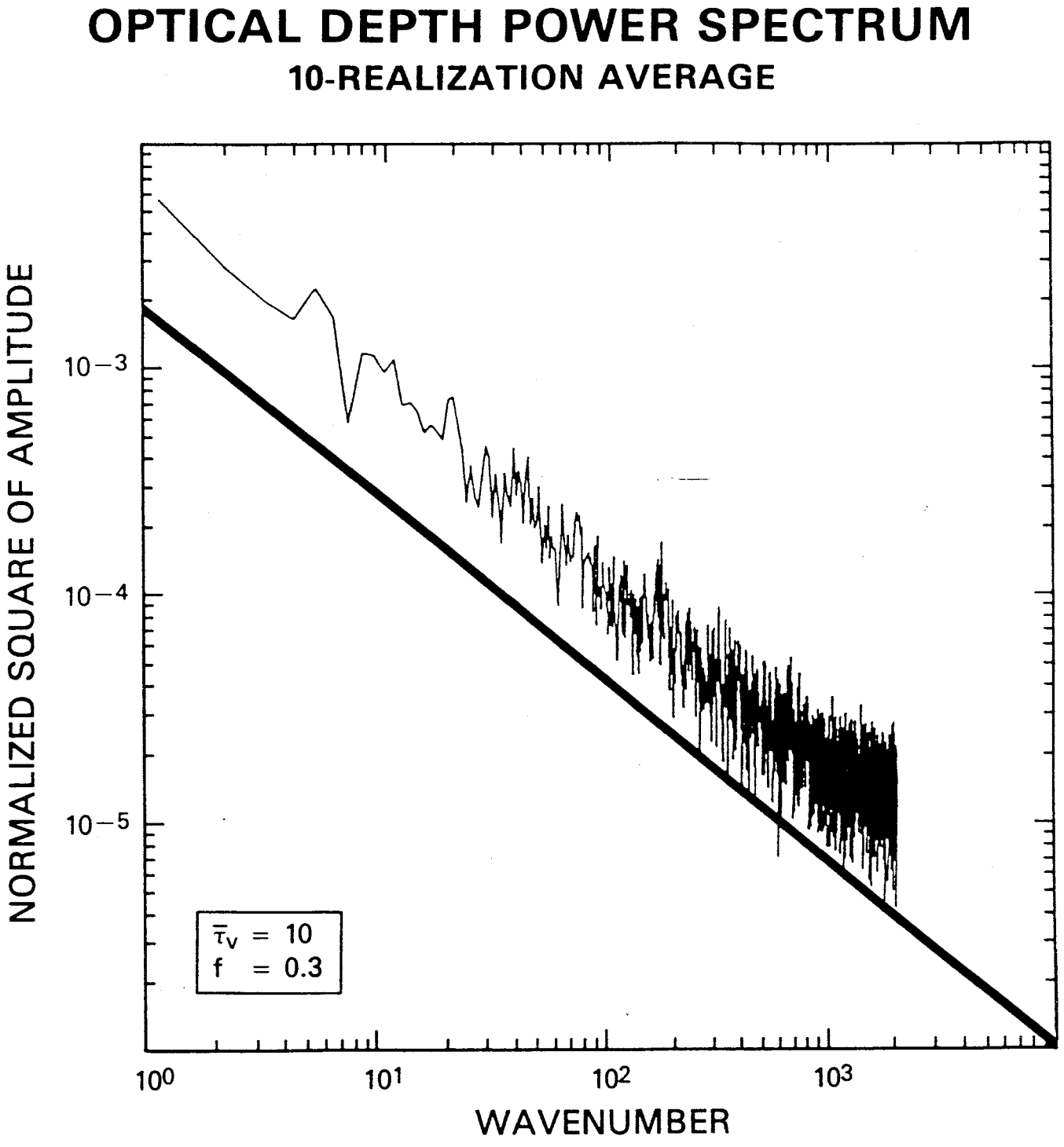

Figure 2. Average wavenumber spectrum of horizontal optical depth variations for 10 realizations similar to that shown in figure 1. The solid straight line corresponds to the theoretical form given by $(\text{wavenumber})^{-0.86}$, where the exponent, determined by (5.8) in the text, is given by $1-[\ln((1+f)/(1-f))/2]^2/\ln 2$ with f=0.3.

random variable with variance var(y). The first n terms in $\ln R_1$ and $\ln R_2$ (before the points are separated) will be identical, and the last N-n will be independent, so that

$$\ln R_1 + \ln R_2 = 2 \sum_{k=1}^{n} x_k + \sum_{k=1}^{2(N-n)} x_k \tag{5.5}$$

This is normally distributed for large N, so that the mean of (5.3) may be found from the identity (5.4), using

$$\mathrm{var}(\ln R_1 + \ln R_2) = 4n\,\mathrm{var}(x) + 2(N-n)\,\mathrm{var}(x). \tag{5.6}$$

The n-dependent part behaves as

$$\langle R_1 R_2 \rangle \sim \exp[n\,\mathrm{var}(x)] \sim (L/d)^{\mathrm{var}(x)/\ln 2}. \tag{5.7}$$

The power spectrum corresponding to the covariance (5.7), given by the Fourier transform, behaves as

$$S \sim k^{-[1-\mathrm{var}(x)/\ln 2]}. \tag{5.8}$$

where k is the wavenumber. This power-law satisfies the relation (2.1) expected of a self-similar scaling fractal. The average spectrum for 10 realizations of the subdivision process is shown on a log-log plot in figure 2, and decreases with a slope given by the exponent in (5.8). The random deviations from this power-law behavior are due to sampling error, and decrease with the square root of the number of realizations.

After carrying out the Monte Carlo computations with the parameters listed above, perhaps the simplest quantity to examine is the horizontally averaged albedo. Figure 3 shows a plot of the average albedo versus N, the number of iterations, for 10 realizations of the subdivision process. The error bars give the albedo range, and the solid line the mean albedo over the 10 realizations. As one subdivides to finer and finer scales, the albedo initially decreases linearly with N, and then approaches a constant after about N=8, where the horizontal optical depth of each segment becomes less than about 10, so that the aspect ratio becomes less than 1.

The linear regime, in which N is small and each segment is horizontally optically thick, can be approximated by computing the albedo of each segment independently as if it were plane-parallel. This approximation is shown as the line labelled "independent pixels" in figure 3. The redistribution of liquid water at each iteration decreases the mean albedo from the plane parallel case, since the albedo of optically thick regions saturates as their optical depth is increased, while the thin regions continue to darken as their optical depth is decreased.

The albedo of each homogeneous region may be computed from the thickness of each region independently only when the horizontal optical depth is large compared to the photon mean free path. As we approach N=8 in figure 3, each segment becomes comparable in horizontal optical depth to the photon mean free path, and the albedo depends upon radiation from the sides of each segment. As we approach the large N asymptotic regime, the mean albedo becomes insensitive to variations in optical depth occuring on horizontal scales much smaller than the photon mean free path, so that further subdivisions produce no further decrease.

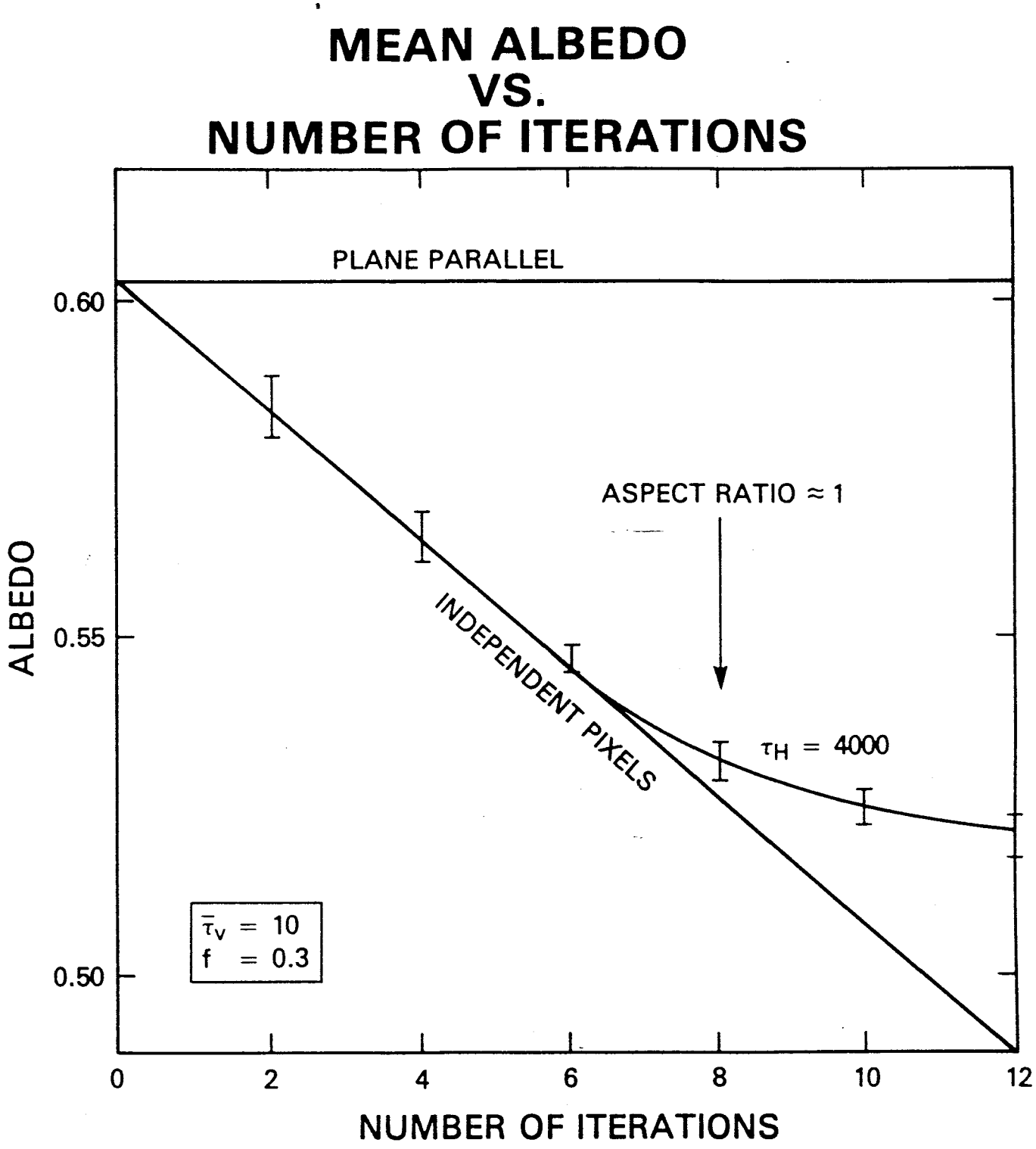

Figure 3. Mean albedo versus the number of iterations of the subdivision process. The error bars give the range of values for 10 realizations. The horizontal line gives the plane-parallel albedo for optical depth = 10. The line labelled "independent pixels" gives the average albedo obtained by setting the albedo of each segment equal to the plane-parallel albedo corresponding to its particular optical depth. As the number of iterations increases, the actual albedo determined by Monte Carlo follows the independent approximation until the horizontal optical depth becomes comparable to the vertical optical depth, which occurs near N=8 (since $4000/2^8 \approx 10$), beyond which the albedo becomes insensitive to further subdivision.

The effect of the photon mean free path on the horizontal variations in albedo may be seen in figure 4, which shows the average power spectrum of the albedo on a log-log plot for 10 realizations of the subdivision process. The large-scale (small k) behavior shows the same type of power-law decrease as the optical depth, while the small scale behavior is independent of k, indicating purely uncorrelated variations, or "white noise".

A feeling for the type of errors made by the linear "independent pixel" approximation can be gained by comparing its horizontal variation with that of the Monte Carlo result for a single realization. For each of the curves in figure 5 the white noise has been filtered out by applying a triangular running mean over the horizontal scale $\tau_h=\pm 50$. The solid curve shows one realization of the Monte Carlo horizontal variation of albedo. The dotted curve shows the independent pixel approximation, in which the albedo is a monotonic function of the local optical depth. It clearly underestimates the albedo in each of the darker regions, near local minima of the optical depth, but provides a good approximation in the brighter regions. This difference is due to the radiation from the sides of the optically thinner regions, which considerably brightens them. Note that the solar radiation, which is incident from the left in the figure, tends to enhance the albedo on the left of each of the optical depth maxima. This solar zenith angle dependence also depends upon the fractal parameter f.

To improve the independent pixel approximation, we must estimate the effect of radiation transferred from the optically thick regions into the thin ones. One way is to employ an "effective" optical depth which depends on the environment of each segment. As a first guess, we simply apply the same ± 50 triangular running mean to the optical depth to obtain an "effective" optical depth. This "filtered independent pixel" approximation is given by the dashed line in figure 5. It provides a clear improvement in the dark regions, and a better estimate of the mean albedo, but does not show the solar zenith angle dependence of the Monte Carlo result.

6. DISCUSSION

We have given a brief overview of work being done at Goddard Space Flight Center and Tel-Aviv University on the fractal properties of clouds and their implications for large-scale radiative properties of the atmosphere. Three examples of relatively simple fractals were described to illustrate concepts needed in modelling fractal cloud structure. The results of empirical studies of cloud structure determined from LANDSAT observations were then summarized, emphasizing the dependence of the fractal parameters on cloud type and threshold. A procedure for simulating the type of structure observed by LANDSAT was described, with a summary of the various parameters involved, and a one-parameter fractal model was introduced, which despite its lack of realism provides a useful tool for the investigation of radiative transfer through fractal clouds. The radiative properties of this "simplest" fractal cloud were summarized, with emphasis on the importance of the optically thin regions, and the role of the photon mean-free-path.

Work along these lines is continuing in our group and elsewhere (see e.g. references by Lovejoy and Schertzer, Rhys and Waldvogel, and Wielicki and Welch). Much remains to be done in terms of understanding the physical basis of fractal cloud structure and the process of radiative transfer through fractal clouds. This improved understanding may lead to improved remote sensing of cloud properties, and better parameterization of clouds in climate models.

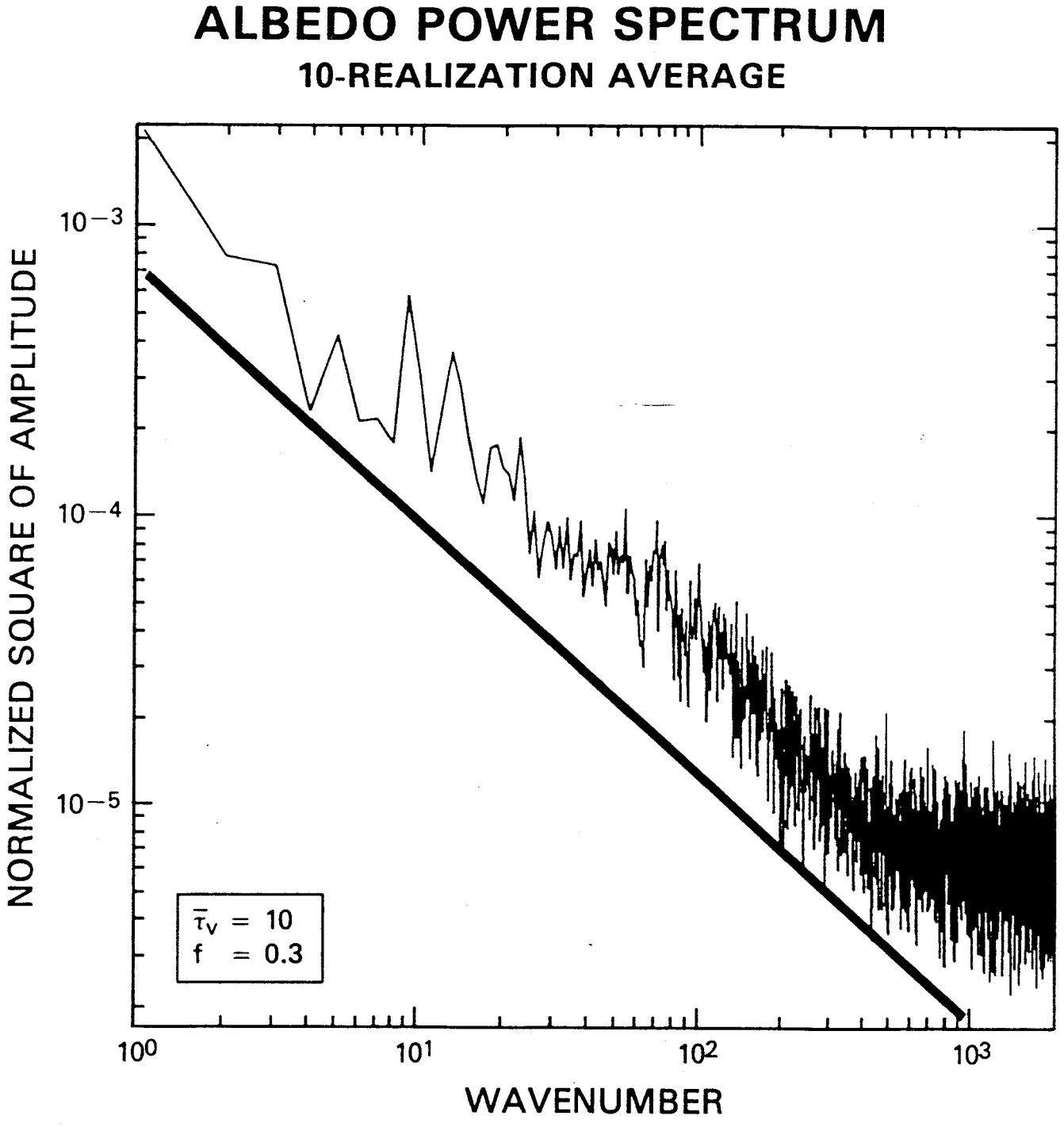

Figure 4. Average wavenumber spectrum of horizontal albedo variations for 10 realizations of albedos computed from optical depth variations like those shown in figure 1. The spectrum initially follows the power law indicated by the straight line, but becomes independent of wavenumber above about 400, which corresponds to horizontal scales smaller than about 10 optical depth units, the same scales to which the mean albedo in figure 3 is insensitive.

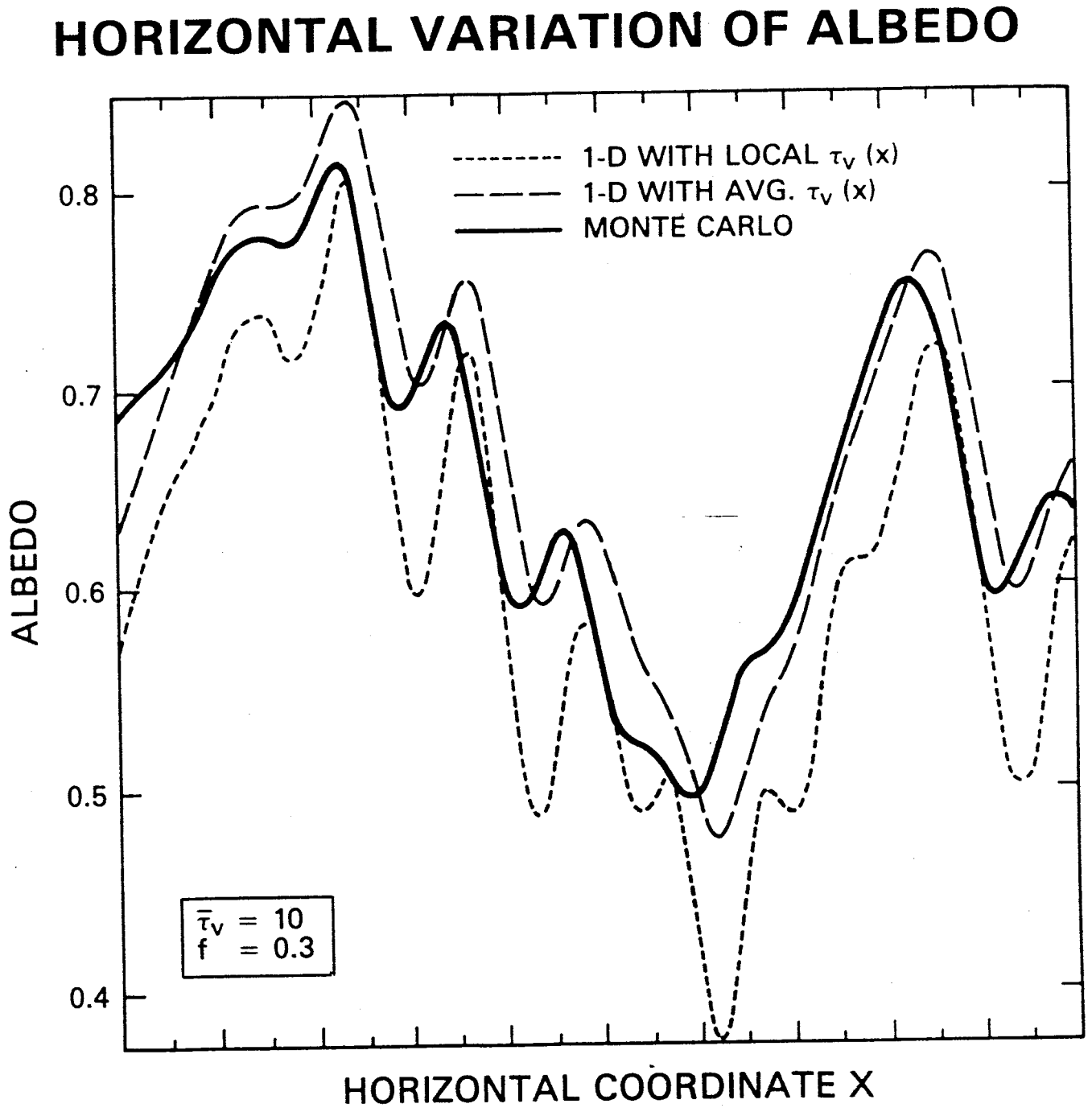

Figure 5. One realization of the horizontal variation of albedo, with the incident solar radiation from the left at a zenith angle of 60°. All three curves have been smoothed over horizontal optical depths of ±50 with a triangular filter. The dotted line is obtained by setting the albedo of each segment equal to the plane-parallel albedo corresponding to its particular optical depth. Thin regions appear very dark in this approximation. The solid line is the Monte Carlo result, which shows the brightening effect of neighboring segments on the thin regions. The dashed line is obtained by setting the albedo of each segment equal to the plane-parallel albedo associated with the average vertical optical depth over the region 50 units on either side. This produces a better approximation to the Monte Carlo result, especially in the thin regions, but tends to overestimate on the downstream side of the thick regions.

REFERENCES

Baker, M. and J. Latham, 1979: The evolution of droplet spectra and the rate of production of embryonic raindrops in small cumulus clouds, *J. Atmos. Sci.*, **36**, 1612-1615.

Cahalan, R. F., 1986: Nearest neighbor spacing distributions of cumulus clouds, Proceeding of the 2nd International Conference on Statistical Climatology, Vienna, Austria, June, 1986.

_____, 1987: LANDSAT observations of fractal cloud structure, in **Scaling, Fractals and Nonlinear Variability in Geophysics**, D. Schertzer and S. Lovejoy, ed., Reidel, in press.

_____, and J.H. Joseph, 1988: Fractal statistics of cloud fields, *Mon. Wea. Rev.*, to appear.

Caughey, S. J., B. A. Crease and W. T. Roach, 1982: A field study of nocturnal stratocumulus II. turbulence structure and entrainment. *Quart. J. R. Met. Soc.*, **108**, 125-144.

Coakley, J. A., Jr., and F. P. Bretherton, 1982: Cloud cover from high-resolution scanner data: detecting and allowing for partially filled fields of view. *J. Geophys. Res.*, **87**, 4917-4932.

Derr, V. and R. Gunter, 1982: EPOCS 1980: Summary Data Report-- Aircraft Measurements of Radiation, Turbulent Transport and Profiles in the Atmospheric and Oceanic Boundary Layers of the Tropical Eastern Pacific, NOAA Tech. Memo. ERL WPL-101, NOAA Wave Propagation Lab, Boulder, Colorado.

Falconer, K.J., 1985: **The Geometry of Fractal Sets,** Cambridge University Press.

Farmer, J. D., E. Ott and J. A. Yorke, 1983: The dimension of chaotic attractors, *Physica*, **7D**, 153-180.

Frisch, U. and O. Parisi, 1985: On the singularity structure of fully developed turbulence. in **Turbulence and Predictability in Geophysical Fluid Dynamics and Climate Dynamics**, M. Ghil, ed., Elsevier Science Publishers B.V., Amsterdam, The Netherlands, pp. 84-88.

Hentschel, H.G.E. and I.Procaccia, 1983: The infinite number of generalized dimensions of fractals and strange attractors. *Physica*, **8D**, 435-444.

_____and_____, 1984: Relative diffusion in turbulent media, the fractal dimension of clouds. *Phys. Rev.*, **A29**, 1461-1476.

Lovejoy, S., 1982: Area-perimeter relation for rain and cloud areas. *Science*, **216**, 185-187.

_____, and B. B. Mandelbrot, 1985 : Fractal properties of rain and a fractal model. *Tellus*, **37A**, 209-232.

_____, and D. Schertzer, 1985 : Generalized scale invariance in the atmosphere and fractal models of rain. *Water Resour. Res.*, **21**, 1233-1250.

Mandelbrot, B. B., 1983: **The Fractal Geometry of Nature**. W. H. Freeman and Co., San Francisco, 460pp..

_____, 1986: Self-affine fractal sets. Parts I., II. and III., in **Fractals in Physics**, L. Pietronello and E. Tosatti, ed., Elsevier Science Publishers B.V., Amsterdam, The Netherlands, pp. 3-28.

Randall, D. A. and G. J. Huffman, 1980: A stochastic model of cumulus clumping. *J. Atmos. Sci.*, **37**, 2068-2078.

Rhys, Franz S., and A. Waldvogel, 1986: Fractal shape of hail clouds. *Phys. Rev. Lett.*, **56**, 784-787.

Schertzer, D. and S. Lovejoy, 1986 : Generalized scale invariance and anisotropic inhomogeneous fractals in turbulence, in **Fractals in Physics**, L. Pietronello and E. Tosatti, ed., Elsevier Science Publishers B.V., Amsterdam, The Netherlands, pp. 457-460.

_____and_____, 1988 : Multifractal simulations and analysis of clouds by multiplicative processes. *Atmospheric Research*, 21, in press.
Shlesinger, M. F., B. J. West and J. Klafter, 1987 : Levy dynamics of enhanced diffusion: application to turbulence, *Phys. Rev. Lett.*, 58, 1100-1103.
Wielicki, B.A. and R.M. Welch, 1986 : Cumulus cloud properties derived using LANDSAT satellite data, *J. Clim. Appl. Meteor.*, 25, 261-276.
Wiscombe, W. J., W. Ridgway and R. F. Cahalan, 1988: Radiative properties of quasi-fractal clouds, Proceedings of Lille Conference.

DISCUSSION

King: You know when you think of ice crystals they are hexagons because they represent a minimum energy configuration of hydrogen and oxygen atoms. My question is, is there anything in the physics of cloud formation, that is, nucleation, condensation, evaporation and so forth, that would lead one to a physical theory that they would obey fractal geometry, or in other words, is fractal geometry a phenomenological theory or is it a physical theory?

Cahalan: There is no physics in what I have talked about here. This is a physics-free description of the liquid water distribution in the cloud. If you try to put in some simple physics like you were talking about and have some sort of a minimum energy configuration, you tend to get clouds that are like soap bubbles. You start out with a bunch of little ones, little ones combine and beget bigger ones and pretty soon your whole region is covered with cloud. On the average, observed cloud fraction tends to be about 50%. The way I think of that is these cells that I was talking about that you are generating the larger ones from have a longer lifetime and you have a largest cell and that has the longest lifetime. If you start generating a bunch of these and let them die after a certain time, you are going to tend to get something like 50% cloud cover from that sort of model. And the physics is what determines the lifetime.

Neuendorffer: It would seem like you might be able to do another step improving it if you increased thickness as well as increase the amount of water. Is that going to be complicated?

Cahalan: So far we just took the simplest theoretical model because we have many parameters to vary and we've been burning CYBER time. But eventually the model will be motivated by the FIRE data analysis of both height and liquid water variations. The Monte Carlo calculations are set up to be able to deal with an arbitrary three-dimensional distribution.

Neuendorffer: It is very interesting work. Are you the only people doing this kind of thing?

Cahalan: Bruce Wielick at NASA/Langley is also doing analysis of LANDSAT data. Shawn Lovejoy at McGill in Montreal is working on radiative transfer theory but using a six flux type of model.

Speaker: I just wondered how confident are you in your Monte Carlo scheme?

Cahalan: We have error bars in this curve of albedo vs. number of cascades. Each of these points is a computation of 80,000 photons in a single realization and we show 10 realizations there. So, that is the spread that you would get and the solid line is just the mean of those.

Westwater: Many turbulence processes have a spectral decay which goes as -5/3rds in wave number. Is there any connection between the slope of that line and fractal dimension?

Cahalan: Originally, Lovejoy suggested that he was getting 4/3rds because if you consider a temperature field having independent Gaussian variations from point to point then areas above a threshold have a fractal dimension of 4/3. However, more recent data analysis finds that there is no single magic number. Different cloud types have different fractal dimensions. So, I think there is going to be more physics in it. The way the cloud forms is going to matter. For example, fair weather cumulus are driven by heating from below, whereas stratocumulus are driven by cooling from above, and have a strong inversion layer capping them. We find a difference in fractal properties between those two cloud types.

Kleespies: Once you have characterized a cloud field with fractal properties have you thought of any way of using the fractal numbers in paramaterizing the radiative transfer and, in particular, the radiation budget?

Cahalan: That is what we are working toward. These results that I showed you with this highly simplified model of the mean albedo depend on the fractal parameter F. If you believe that type of model (and actually it might apply in certain cirrus situations where you have long streaks of various optical depths) then, you can parameterize large-scale average albedo in terms of the single parameter F. But for other cloud types I think that the average albedo will depend upon additional parameters characterizing such things as cloud spacing and cloud height.